Supplement of Weather Clim. Dynam., 6, 807–816, 2025
https://doi.org/10.5194/wcd-6-807-2025-supplement


*Supplement of*

# Linking weather regimes to the variability of warm-season tornado activity over the United States

**Matthew Graber et al.**

*Correspondence to:* Zhuo Wang (zhuowang@illinois.edu)

## Supplementary

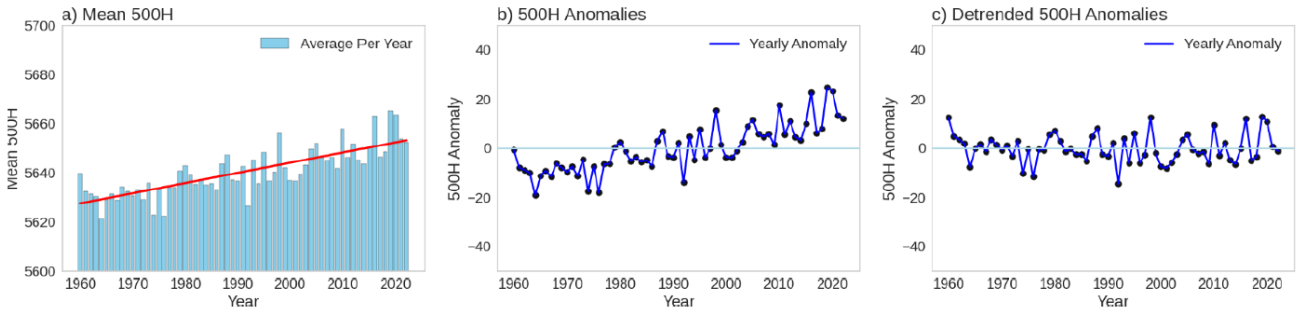


**Fig. S1:** Seasonal 500 hPa geopotential heights averaged over the warm-season (April-July) and Northern Hemisphere. a) Seasonal trend of 500H; b) Seasonal 500H anomalies over time with y = 0 representing the mean; c) Detrended 500H anomalies over time.

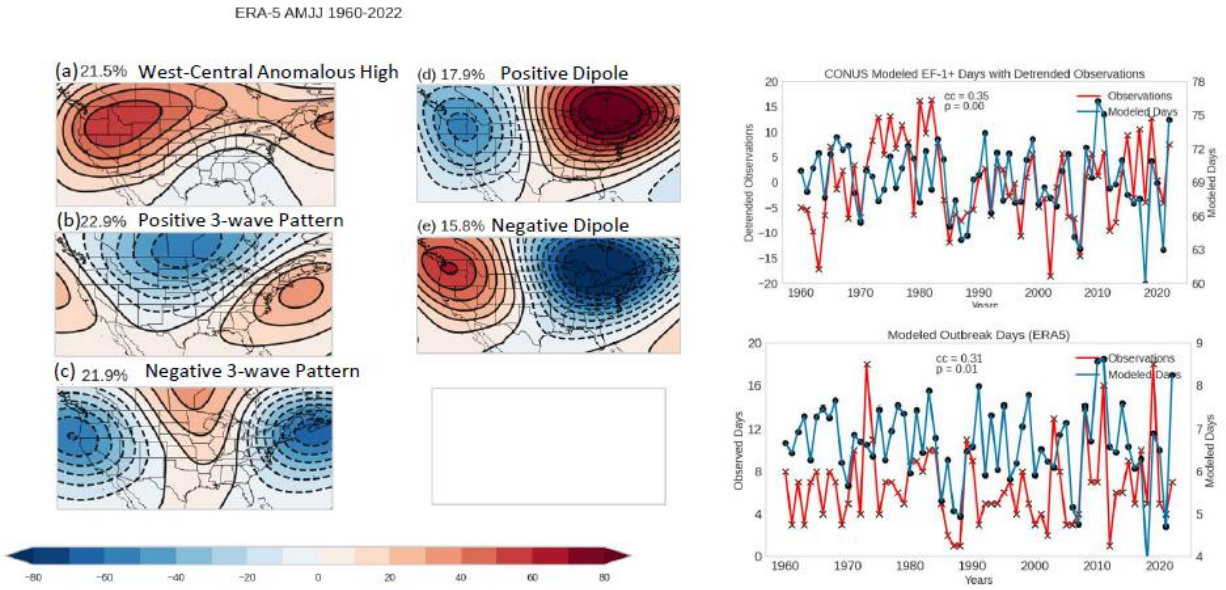


**Fig. S2**: Daily Mean WRs and empirical modeling with no filtering

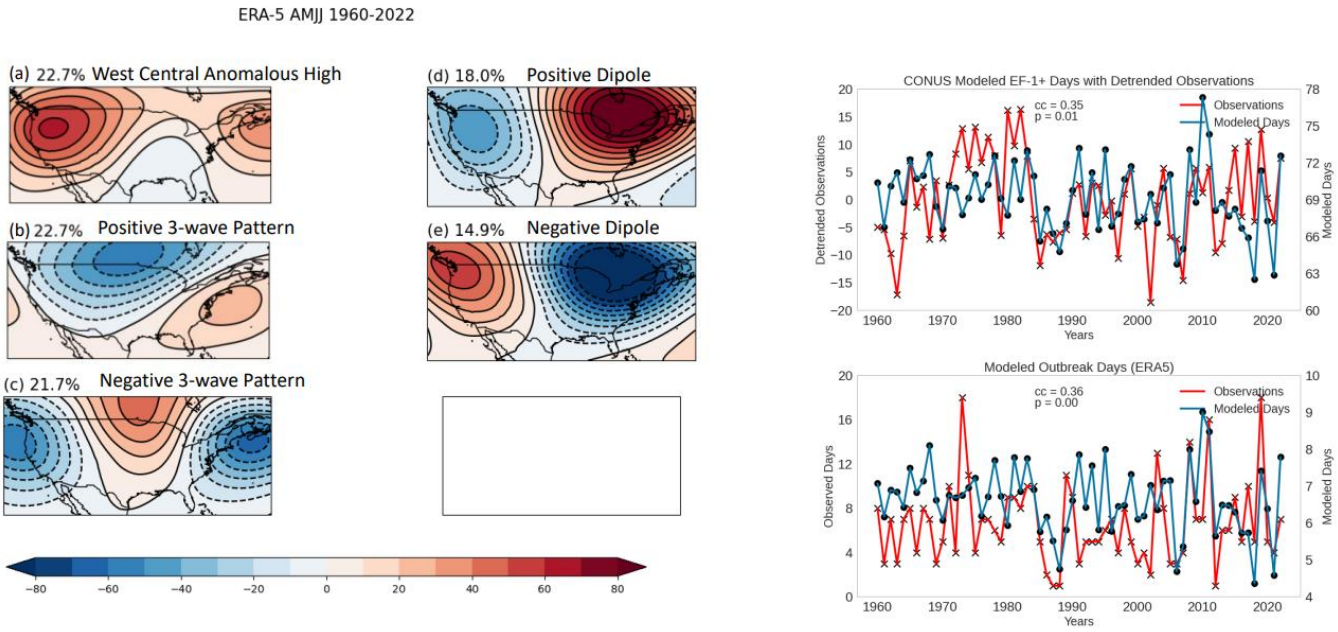


**Fig. S3:** Daily Mean WRs and empirical modeling with a 5-day low-pass filter

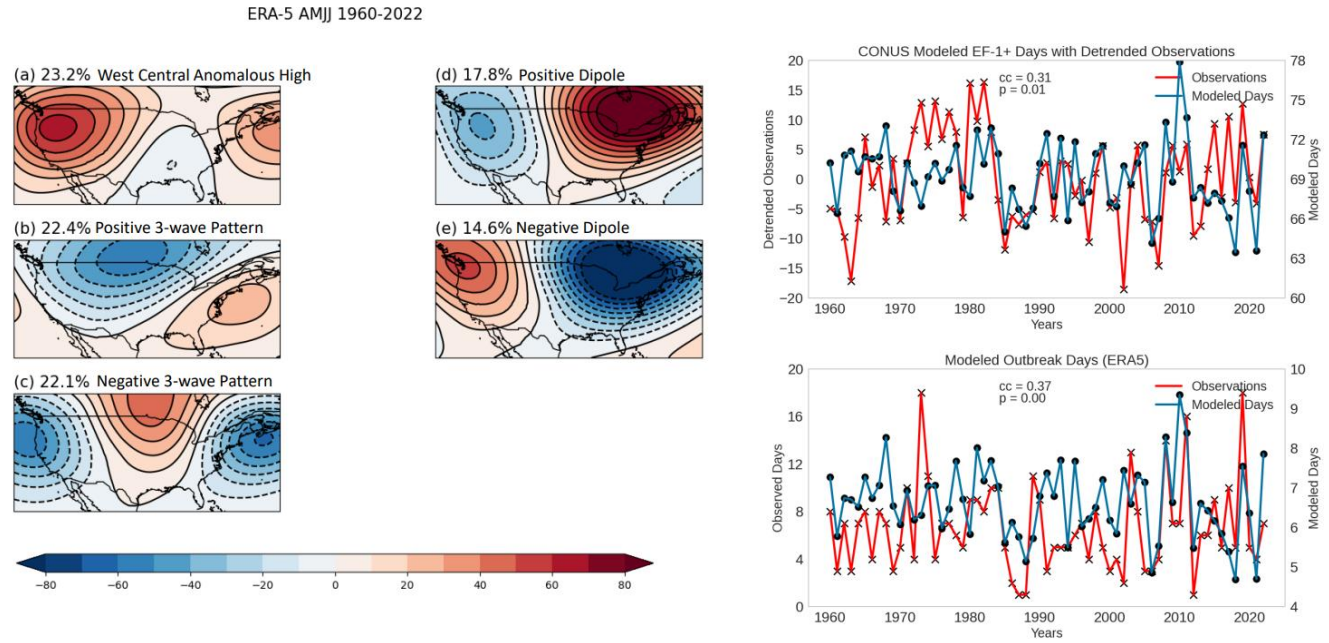


**Fig. S4:** Daily Mean WRs and empirical modeling with a 5-day low-pass filter and EOF dimension reduction (WRs used in main manuscript).

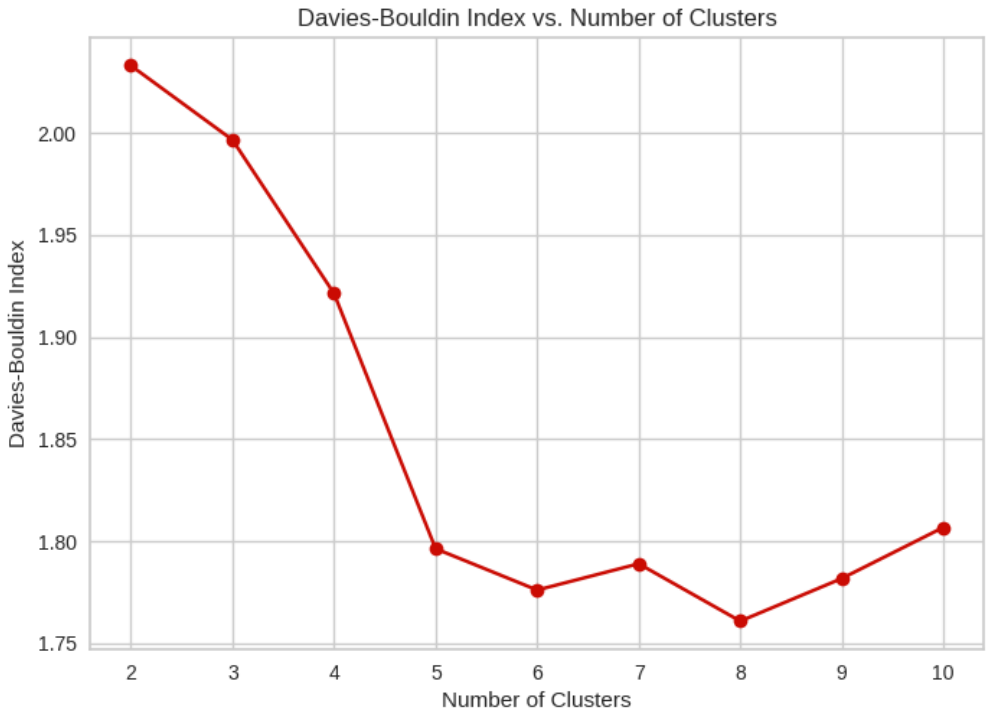


**Fig. S5:** Davies Bouldin Index for each number of clusters.

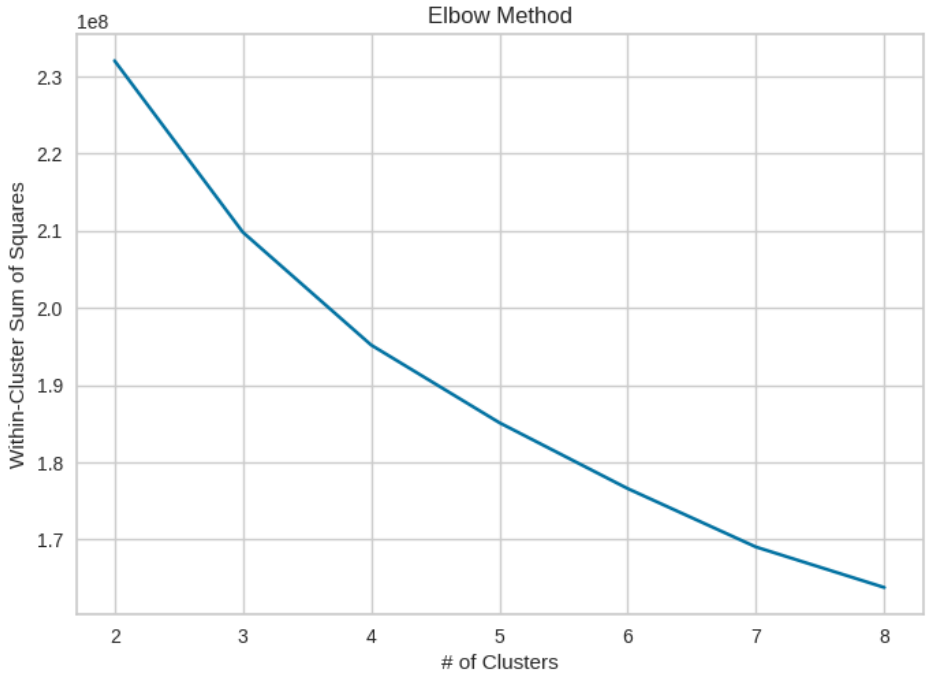


**Fig. S6:** Elbow method for each number of clusters.

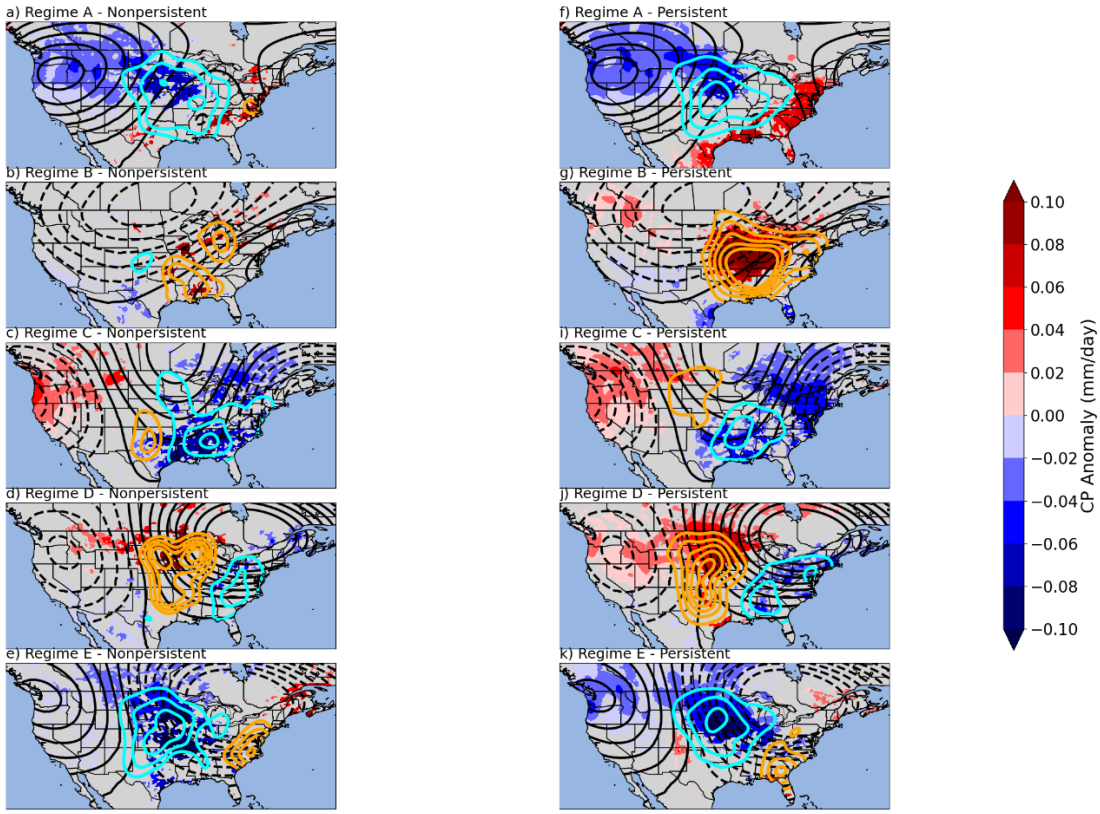


**Fig. S7:** Non-persistent (left column) and persistent (right column) composite anomalies of convective precipitation (shaded) and TD probabilities (contours). A gaussian filter with sigma 8 is applied to TD probability anomalies and a 2x2$^{o}$ uniform filter is applied to the convective precipitation anomalies to smooth them. Significance ($p<0.05$) is tested at each grid point using a one-sample, two-sided t-test to mask out non-significant anomalies.

| Regime | Total Nonpersistent WR Days | Nonpersistent WR Days with a TO | Total Persistent WR Days | Persistent WR Days with a TO |
|---|---|---|---|---|
| A | 509 | 9 | 1272 | 29 |
| B | 494 | 37 | 1226 | 128 |
| C | 471 | 18 | 1228 | 51 |
| D | 398 | 29 | 967 | 73 |
| E | 268 | 12 | 853 | 32 |

**Table S1** Counts of total non-persistent and persistent WR days.

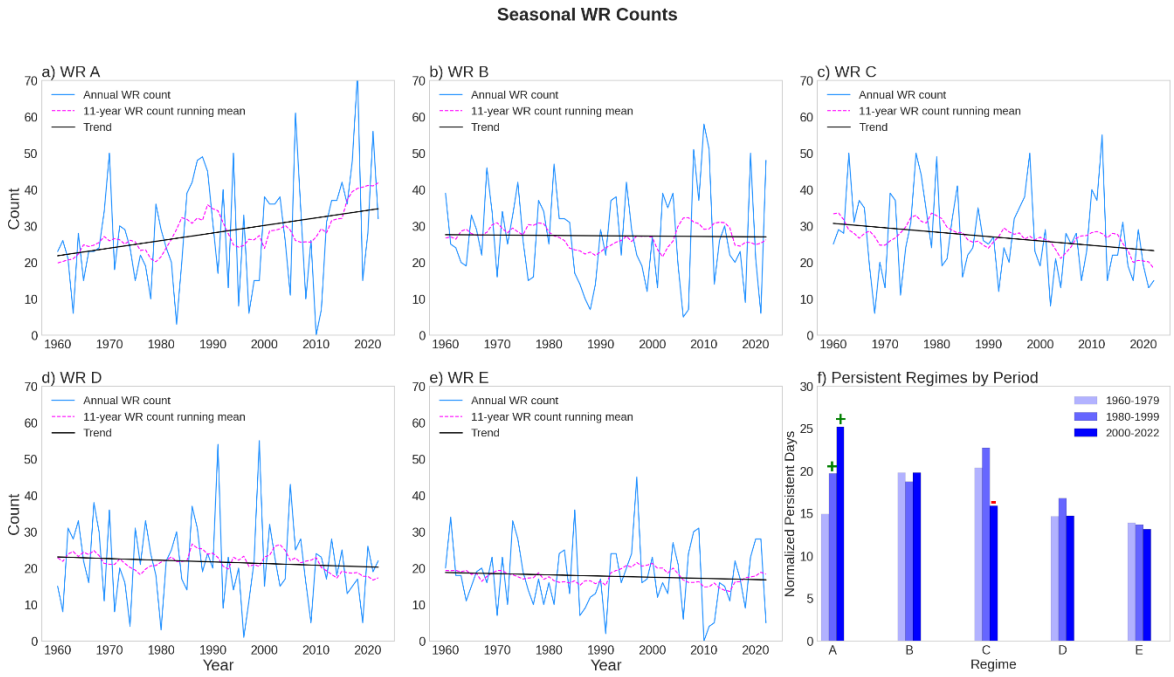


**Fig. S8**:-a-e) Seasonal WR counts, 11-year WR count running mean, and 63-year trend; f) Persistent regime days per period normalized by number of years in each period. +'s and – 's indicate significant increases and decreases from the previous period, respectively, using Student's t test (≥ 95 % confidence).

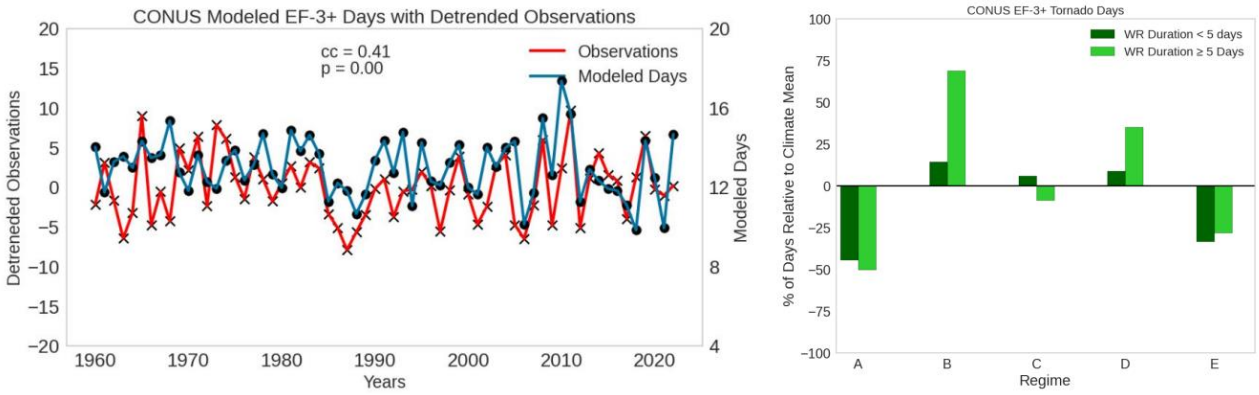


**Fig. S9:** The modeled EF-3+ days (blue) during 1960-2022 along with the detrended EF-3+ days from observation (red). The Spearman rank correlation coefficient (CC) and p-value of the two time series are also shown. On the right are the TD probability anomalies associated with this simulation.

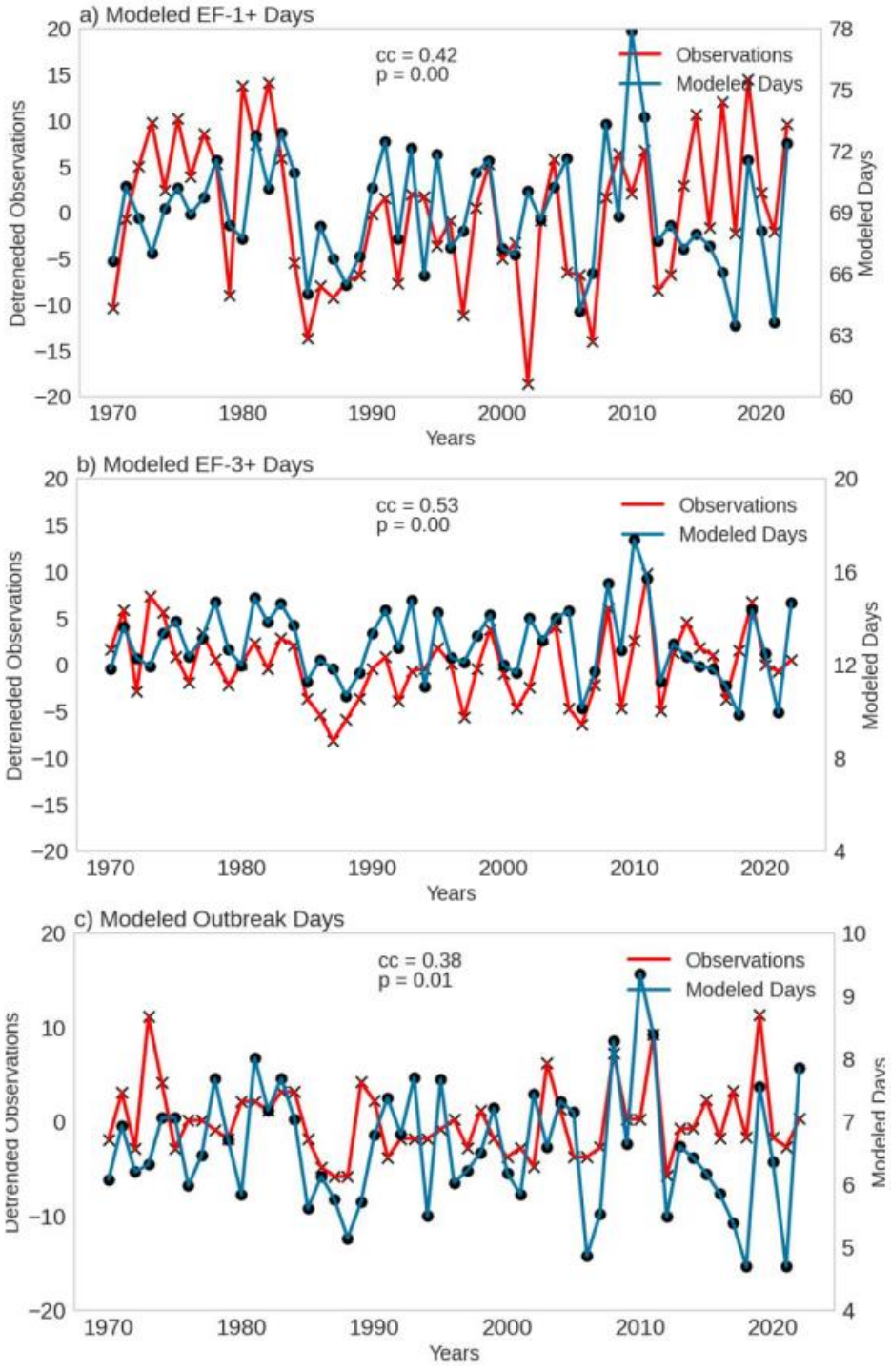


**Fig. S10:** The modeled (blue) and the observed (detrended, red) tornado indices during 1970-2022, along with the corresponding Spearman rank correlation coefficient (CC) and p-value.

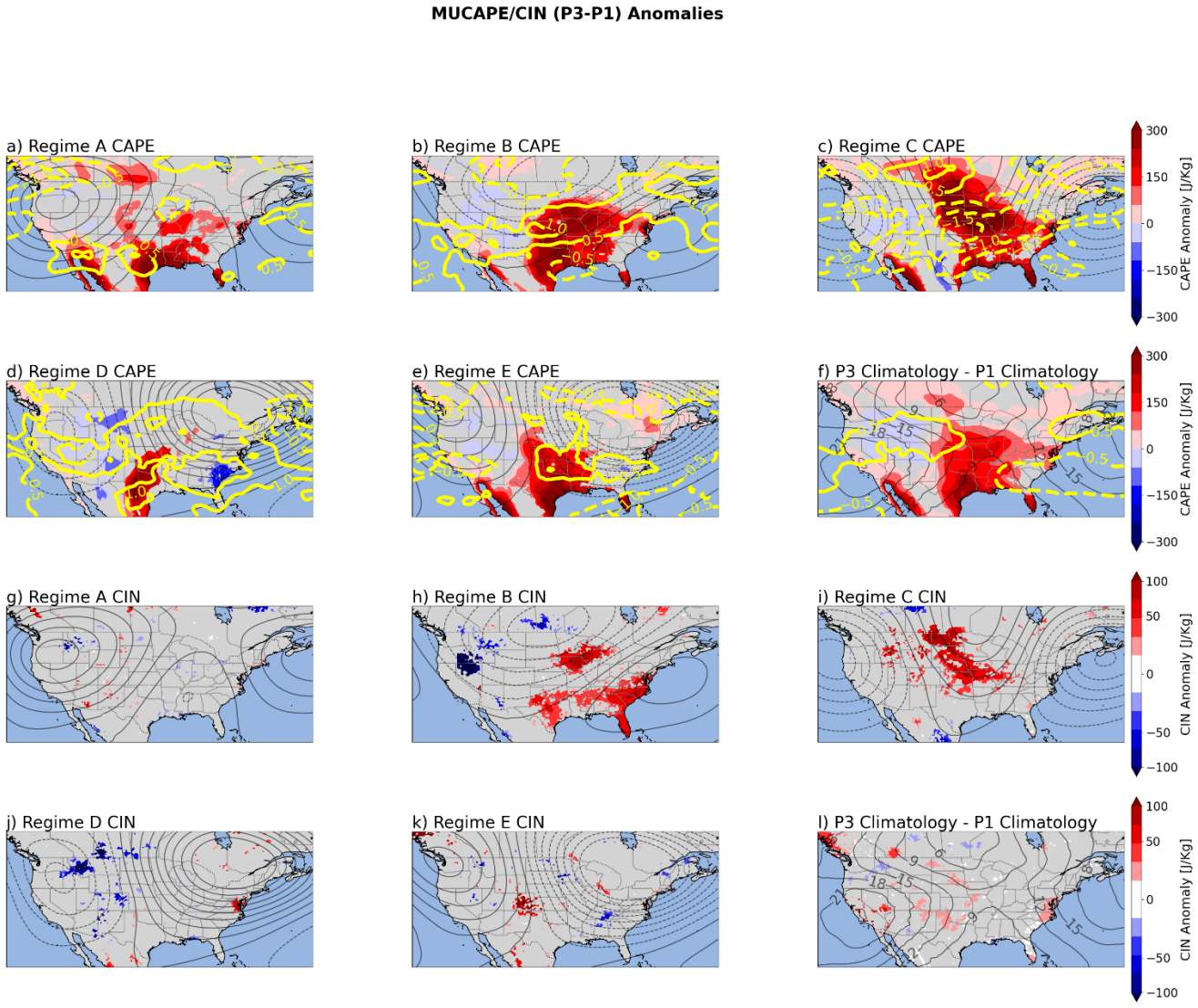


**Fig. S11:** Change in MUCAPE (shading) and S06 (contours) (a-e) and CIN (shading) (g-k) from period 1 (1960-1979) to period 3 (2000-2022) for each WR and (f, l) all WR days at each grid point. A two-sample, two-sided t-test was used to only plot significant ($p<0.05$) anomalies. A gaussian filter with sigma 4 was applied to the CIN anomalies to account for the reduced sample size and make the data less noisy.